CHAPTER 5

Nickel silicide and nickel germanosilicide based Ohmic contacts on $Si_{1-x}Ge_x$

In this chapter we present the material and electrical properties of nickel germanosilicide formed on the variious $Si_{1-x}Ge_x$ (x=0, 0.2 and 0.3) layers, such as formed phase, formation of agglomerates, sheet resistance and specific contact resistivity. Besides, thermal stability of nickel germanosilicide on high-dose B^+, BF_2^+, P^+ and As^+ -implanted $Si_{0.8}Ge_{0.2}$ epilayers was investigated by sheet resistance measurements. The Si capping layer grown on top of the $Si_{1-x}Ge_x$ layers for improving the quality of silicidation films are adopted in this study. In the second part of the chapter, the agglomeration occurred in the silicidation film is suppressed and the electrical property is improved by introducing a suitable thickness of Si capping layers. In addition, the morphological stability of the nickel germanosilicide after aging at the temperature of 400℃ is also discussed.

5-1 Introduction

Silicided strained $Si_{1-x}Ge_x$ junction has attracted lots of attention because of its potential applications to band-gap engineering by varying the Ge fraction in the $Si_{1-x}Ge_x$ layer. Some of its potential applications include serving as the base of heterojunction bipolar transistors [1] and the raised source/drain in deep submicron metal-oxide-semiconductor transistors. Concurrently, metal silicides have been widely employed in ultra large scale integrated (ULSI) circuits as contacts and gate electrodes. For sub-100-nm technology node, $CoSi_2$ is expected to be further replaced by NiSi. NiSi has several advantages over $TiSi_2$ and $CoSi_2$ for the ultra-small CMOS process. They are (1) low temperature silicidation process, (2) low silicon consumption, (3) no bridging failure property, (4) smaller mechanical stress, (5) no adverse narrow line effect on sheet resistance, and (6) smaller contact resistance for both n- and p-Si [2]. These advantages are also for $Si_{1-x}Ge_x$ semiconductor. Significant efforts have thus been

made in understanding the phase formations and properties of the metal/$Si_{1-x}Ge_x$ reactions [3,4]. Among the potential metal silicides, nickel silicide is particularly attractive because of its low resistivity, cubic crystal structure, relatively small lattice mismatch with Si, and the compatibility with self-aligned silicide scheme. In addition, in practical applications the thermal stability of nickel germanosilicides on high-dose ion-implanted $Si_{1-x}Ge_x$ at temperatures compatible with the device fabrication process is of critical importance. In previous studies, strong effects of BF_2^+ and Si^+ implantation on the growth of polycrystalline $NiSi_2$ on silicon were observed [5-7], but the detailed materials of reactions of germanosilicides on $Si_{1-x}Ge_x$ needs further study. For conventional furnace annealing the formation of a ternary phase was generally accompanied with Ge segregation. Rapid thermal annealing (RTA) can shorten the annealing time, resulting in a reduction of Ge segregation. Furthermore, RTA can produce an excellent silicide film without inducing strain relaxation in the unreacted $Si_{1-x}Ge_x$ film. In this section, we investigated the electrical and material properties of the nickel germanosilicide contact. The germanosilicide formed on P^+-$Si_{0.8}Ge_{0.2}$ layer shows the low sheet resistance of 6.85-7.57Ω/□, which is smaller than that of the nickel germanosilicide formed on P^+-$Si_{0.7}Ge_{0.3}$ layer. Low contact resistance of less than 9.7×10^{-7}Ω-cm^2 is achieved for nickel germanosilicide on P^+-$Si_{0.91}Ge_{0.09}$ sample. The superior electrical characteristics of the nickel germanosilicide on P^+-$Si_{1-x}Ge_x$ layer are attributed to the uniform thickness, smooth surface and the smooth interfaces between the silicide and the underlying $Si_{1-x}Ge_x$ layer. The thermal stability of the nickel germanosilicide was significantly affected by the implantation species in $Si_{0.8}Ge_{0.2}$ epilayers and BF_2^+ is superior among them. In high-dose B^+, P^+ and As^+-implanted samples, agglomeration of nickel germanosilicide become very severe after 800℃, 30s rapid thermal annealing. However, in high-dose BF_2^+-implanted samples the agglomeration of nickel germanosilicide is lower than using other implantation species. This is attributed to the retardation of the formation of agglomeration by the presence of fluorine dose in the nickel germanosilicide layers.

In this research, we also investigated the electrical and material properties of the nickel silicide formed by depositing nickel on Si/P^+-$Si_{1-x}Ge_x$ and annealed by RTA method and compared the properties with that of the nickel germanosilicide formed by direct deposition of nickel on P^+-$Si_{1-x}Ge_x$ without Si intermediate layer. In addition, the morphological stability of the nickel silicide Ohmic contact in comparison with the nickel germanosilicide Ohmic contact requires further investigation. The thermal stability of the silicide films formed on Si/$Si_{0.8}Ge_{0.2}$ and $Si_{0.8}Ge_{0.2}$ as Ohmic contacts and compares the electrical and material characteristics of these silicide Ohmic contacts following aging at sintering temperature of 400℃ for 48 hours were investigated in this research.

5-2 Experimental procedures

N-type 6 inch (100) silicon wafers with 10-15 Ωcm sheet resistance were used as the starting substrates. Strained $Si_{1-x}Ge_x$ thin films with x=0.09, 0.14, 0.2 and 0.3 were grown on these wafers by an ultrahigh vacuum chemical molecular epitaxy (UHVCME) system [8]. Wafers were first subjected to a pre-clean process before loading into the loading chamber. After that, the wafers were immediately transferred to the growth chamber and heated to 850 ℃ for 500 s for further cleaning of the Si surface. For the growth of the *in-situ* boron-doped $Si_{1-x}Ge_x$ layers, pure GeH_4, Si_2H_6, and 1% B_2H_6 diluted with H_2 were introduced into the growth chamber to achieve a boron concentration of $2\times10^{19}cm^{-3}$ in all cases. For the P^+-$Si_{1-x}Ge_x$ layer samples, the thickness of the $Si_{1-x}Ge_x$ epitaxial layer was 100 nm. Wafers with grown P^+-$Si_{1-x}Ge_x$ layers were then cleaned by a standard clean procedure, and dipped in 10% HF solution for 30 sec to remove the native oxide. For thermal stability study, following a standard cleaning procedure, the $Si_{1-x}Ge_x$ epi-wafers were implanted with 25 keV BF_2^+, 25 keV B^+, 30 keV P^+ and 30 keV As^+ (all species to a dose of $5\times10^{15}/cm^2$). A 15-nm-thick nickel film was then deposited by the Metal-PVD on these epitaxial wafers. Next, a 5-nm-thick TiN cap layer was deposited on the top of the nickel film to prevent nickel

oxidation during the silicidation process. The Ni-P^+-$Si_{1-x}Ge_x$ silicidation reactions were then performed in an RTA system with nitrogen ambient for 30sec with different annealing temperatures. After silicidation process, the TiN-capping layer and the unreacted Ni film were selectively removed by wet etching in 4 H_2SO_4 : 1 H_2O_2 (30%) solution for 5 min. To test the stability of these contacts, the nickel silicide and nickel germanosilicide Ohmic contacts were aged in a furnace at sintering temperature (400℃) for up to 48 hours in a nitrogen ambient. The sheet resistance R_S was measured by a conventional four-point probe measurement system. Measurement of the contact resistance R_C was performed using the transmission line model (TLM). The analysis of the material structures and the morphologies of the silicides were investigated by cross-sectional transmission electron microscopy (TEM) and scanning electron microscopy (SEM). The compositions of the materials were characterized by energy dispersive spectrometry (EDS). Auger electron spectroscopy (AES) was used to determine the chemical depth profiles of Ni, Si, Ge, and O.

5-3 Material properties of the Ni/$Si_{1-x}Ge_x$ thin films

Figure 5.1 shows the XRD spectra of the nickel germanosilicide films annealed at the temperature from 350 to 750℃ for 30 sec. Figure 5.1 (a) shows the Ni_2 ($Si_{1-x}Ge_x$) peaks of the 350℃ annealed sample were (020) and (110), respectively. The XRD spectra indicates the formed phase of the silicidation film is $Ni_2(Si_{1-x}Ge_x)$ after annealing at 350℃ for 30 sec. After annealing at 500℃ for 30 sec the $Ni_2(Si_{1-x}Ge_x)$ phases were transformed to $Ni(Si_{1-x}Ge_x)$ phases at (101), (201) and (004) peaks were observed as shown in Fig.5.1 (b). As the silicidation temperature was increased to 750℃, the XRD spectra show that the formed phase is $Ni(Si_{1-x}Ge_x)_2$ and the orientation is the diffracted peak of (111) as shown in Fig.5.1 (c).

The compositional properties analyzed by AES measurements are shown in Fig. 5.2. It can be seen that no oxygen pile-up was observed in nickel germanosilicide films formed on both $Si_{0.8}Ge_{0.2}$ and $Si_{0.7}Ge_{0.3}$ layers after annealing at 500℃ for 30 sec as shown in Fig.5.2 (a)

and (b). No formation of silicon and nickel oxides was observed in the nickel germanosilicide film which was due to the deposition of 5-nm thick TiN capping layer on top of the nickel film. The results also indicate that the phase formed in the Ni/$Si_{0.8}Ge_{0.2}$ and Ni/$Si_{0.7}Ge_{0.3}$ samples are all mono-nickel germanosilicide after annealing at 500℃ for 30 sec. In addition, the Ge segregation effect was not observed in both Ni/$Si_{0.8}Ge_{0.2}$ and Ni/$Si_{0.7}Ge_{0.3}$ samples after annealing at 500℃ for 30 sec. This indicates that nickel germanosilicide films are morphological stability after RTA annealing at this thermal budget.

Figure 5.3 (a) and (b) are the SEM micrograph of the surface morphology of the Ni/P^+-$Si_{0.8}Ge_{0.2}$ and Ni/P^+-$Si_{0.7}Ge_{0.3,}$ respectively after annealing at 500℃ for 30 sec. In both SEM micrographs the white regions were characterized by EDS identified as nickel germanosilicide agglomeration. The grain sizes of the nickel germanosilicide agglomerates (0.3μm) and the micro-voids (0.2μm) are much larger in the Ni/P^+-$Si_{0.7}Ge_{0.3}$ sample than in the Ni/P^+-$Si_{0.8}Ge_{0.2}$ sample (grain sizes=0.1μm and micro-voids=0.12μm). Besides, the surface coverage of the nickel germanosilicide in the Ni/P^+-$Si_{0.8}Ge_{0.2}$ sample (85%) is better than that of the Ni/P^+-$Si_{0.7}Ge_{0.3}$ sample (70%). This is due to more nickel germanosilicide agglomerate and the micro-void formation in the P^+- $Si_{1-x}Ge_x$ samples as the Ge mole fraction increases as observed by the SEM analysis. These phenomena are attributed to the lower heat formation for metal-Ge than for metal-Si [9].

Cross-sectional TEM was used to investigate the material structures of the nickel germanosilicide formed. Figures 5.4 (a) and (b) show the nickel germanosilicide formed on P^+-$Si_{0.8}Ge_{0.2}$ and P^+-$Si_{0.7}Ge_{0..3}$ samples respectively after annealing at 500℃ for 30 sec. The nickel germanosilicide formed on P^+-$Si_{0.8}Ge_{0.2}$ sample after annealed at 500℃ for 30 sec exhibits relatively uniform thickness and smooth interface. In contrast, rough interface and nickel germanosilicide agglomeration are observed in the nickel germanosilicide formed on P^+-$Si_{0.7}Ge_{0.3}$ sample after annealed at 500℃ for 30 sec, the results are consistent with the SEM analysis as shown in the Fig.5.3. The thickness of the Ni/$Si_{0.8}Ge_{0.2}$ and Ni/$Si_{0.7}Ge_{0.3}$

films were 25nm and 23nm respectively after annealing at 500℃ for 30 sec. This means that Ge hinders nickel reaction with Si in the $Si_{1-x}Ge_x$ layer.

5-4 Electrical property of $Ni/Si_{1-x}Ge_x$ thin films

Figure 5.5 shows the R_S of nickel germanosilicide on P^+-$Si_{1-x}Ge_x$. The R_S of nickel silicide on pure p-type Si is also shown in Fig.5.5 for comparison. For the films annealed under the temperature of 350-750℃ for 30 s, the silicidation films were formed. After annealing at temperature of 450-650℃ for 30 s, the P^+-$Si_{0.8}Ge_{0.2}$ sample exhibits superior R_S than that of the P^+-$Si_{0.7}Ge_{0.3}$ sample. Its R_S was 6.85-7.57Ω/□. Compared with Fig.5.3 (a) and (b), it can be seen that as the Ge mole fraction in the $Si_{1-x}Ge_x$ film increased, the grain size of the nickel germanosilicide agglomerates and micro-voids also increased, which is a reason why the R_S of the $Ni/Si_{0.7}Ge_{0.3}$ annealed sample is larger than that of $Ni/Si_{0.8}Ge_{0.2}$ annealed sample. As the silicidation temperature was increased to 750℃, both the $Ni/Si_{0.8}Ge_{0.2}$ and $Ni/Si_{0.7}Ge_{0.3}$ samples formed the $Ni(Si_{1-x}Ge_x)_2$ phase. This is one of the reasons why the R_S of $Ni/Si_{0.8}Ge_{0.2}$ and $Ni/Si_{0.7}Ge_{0.3}$ samples increased abruptly.

The contact resistances Rc of the $Ni/Si_{1-x}Ge_x$ contacts (x=0.09, 0.2, 0.3) formed are shown in Fig.5.6. The R_C increases as the Ge mole fraction increases from 0.09 to 0.3. A minimum R_C value of 0.97 μΩ-cm^2 is observed for the P^+-$Si_{0.91}Ge_{0.0.9}$ sample. However, the R_C value jumps to a higher value for a high Ge mole fraction of 0.3. This is believed to be due to rough interface between the nickel germanosilicide film and $Si_{1-x}Ge_x$ layer. Another reason is larger grain size of nickel germanosilicide agglomerates with increasing number were formed on the surface of the P^+-$Si_{0.7}Ge_{0.3}$.

Figures 5.7 shows R_S data as a function of annealing temperature for BF_2^+, B^+, P^+ and As^+-implanted $Si_{0.8}Ge_{0.2}$ samples. It is apparent that BF_2^+ is most effective in stabilizing the nickel germanosilicide films with lowest R_S at high temperature. The surface morphology of the $Ni(Si_{0.8}Ge_{0.2})_2$ was found to be significantly influenced by the presence of implantation

species in $Si_{0.8}Ge_{0.2}$ layer. The degradation of surface morphology is correlated with the presence of high dose of implantation species. The root mean square (RMS) of the BF_2^+, B^+, P^+ and As^+-implanted nickel germanosilicide surfaces were 2.264, 2.406, 2.489 and 6.351nm, respectively as shown in Fig.5.8. The high dose of BF_2^+ impurities in the $Si_{0.8}Ge_{0.2}$ layer may hamper the reaction of $Ni(Si_{0.8}Ge_{0.2})_2$. For BF_2^+-implanted sample, the presence of fluorine bubbles at the grain boundaries was found to retard the growth of $NiSi_2$ grains on Si [10]. This phenomenon was also observed in the $Ni(Si_{0.8}Ge_{0.2})_2$ grains and needs further investigation. The germanosilicide/$Si_{0.8}Ge_{0.2}$ interface energy and /or germanosilicide surface energy may be altered by the presence of high dose of the implantated species [11]. The presence of B^+ and F^+ alone in $Si_{0.8}Ge_{0.2}$ was found to be not sufficient to maintain 85% surface coverage of $Ni(Si_{0.8}Ge_{0.2})_2$ after 900℃ annealing. The findings seem to suggest a synergetic effect of B^+ and F^+ in retarding the degradation of the $Ni(Si_{0.8}Ge_{0.2})_2$ morphology.

5-5 Material and electrical properties of Ni/Si/$Si_{1-x}Ge_x$ Ohmic contacts

Figure 5.9 compares the sheet resistances (Rs) of the nickel silicide formed on Si/P^+-$Si_{0.8}Ge_{0.2}$ and the nickel germanosilicide formed on P^+-$Si_{0.8}Ge_{0.2}$. The R_S of the nickel silicide on pure P-Si is also shown for comparison. As can be seen in Fig.5.9, when the samples were annealed at 450℃-650℃ for 30 sec, the nickel silicide formed on the Si/P^+-$Si_{0.8}Ge_{0.2}$ sample exhibits superior R_S than that of the nickel germanosilicide formed on the P^+-$Si_{0.8}Ge_{0.2}$ sample. Its R_S is 4.75-5.75Ω/□, which is similar to that of the nickel silicide formed on P-Si. Additionally, the thermal stability of the silicide degrades as the nickel thickness decreases, because the thinner nickel film can easily be consumed to form NiSi during its silicidation process, and NiSi will convert into $NiSi_2$ when annealed at the elevated temperatures. In our experiments, 15-nm nickel was used; the temperature stability of the silicide formed is lower than that of the silicide film formed with thicker nickel film as

reported in Refs [12], [13]. From the SEM (Fig. 5.10 (a), (b)) and cross-sectional TEM images (Fig. 5.10 (c), (d)), we can observe that the nickel silicide formed on the Si/P^+-$Si_{0.8}Ge_{0.2}$ sample lacks agglomeration, and the layer of nickel silicide was very uniform. However, the nickel germanosilicide formed on the P^+-$Si_{0.8}Ge_{0.2}$ sample showed severe agglomeration and micro-voids, and the layer of the nickel germanosilicide was very rough. The EDS/cross-section TEM analysis indicates that the agglomerate is $Ni_2(Si_{1-y}Ge_y)$ as shown in Fig. 5.10 (d). However, the mechanism for the formation of $Ni_2(Si_{1-y}Ge_y)$ agglomeration needs further investigation. This is why the nickel silicide formed on the Si/P^+-$Si_{0.8}Ge_{0.2}$ sample has a lower R_S than the nickel germanosilicide formed on the P^+-$Si_{0.8}Ge_{0.2}$ sample. As the silicidation temperature was increased to 750℃, the formation of $Ni(Si_{1-y}Ge_y)_2$ phases along with the formation of agglomerates with micro-voids cause the increase in the R_S value for the P^+-$Si_{0.2}Ge_{0.8}$ sample as shown in Fig. 5.9. Figure 5.11 shows R_S of the nickel silicide and the nickel germanosilicide as a function of the Ge mole fraction in the $Si_{1-x}Ge_x$ layer after RTA process at 500℃ for 30 sec. The R_S value of the nickel germanosilicide increases significantly as the Ge mole fraction in the P^+-$Si_{1-x}Ge_x$ layer increases. This is due to more nickel germanosilicide agglomerate and micro-void formation in the P^+- $Si_{1-x}Ge_x$ samples as the Ge mole fraction increases as observed by the SEM. These phenomena are attributed to the lower heat formation for metal-Ge than for metal-Si [14]. For the Si/P^+-$Si_{1-x}Ge_x$ samples, the R_S increases slightly as the Ge fraction increases. From our SEM observations, nickel germanosilicide agglomeration starts to occur in theses samples as the Ge fraction increases. This indicates that, for the samples with higher Ge fraction, the thickness of the Si cap layer must be increased to avoid nickel germanosilicide agglomeration. The specific contact resistivity ρ_C of these contacts were also measured. A low ρ_C value of 0.42 μΩ-㎝^{2} was observed for the Si/P^+-$Si_{0.8}Ge_{0.2}$ sample. Meanwhile, the ρ_C for the P^+- $Si_{0.8}Ge_{0.2}$ contact was 3.25 μΩ-㎝^{2} which was much high than the Si/P^+- $Si_{0.8}Ge_{0.2}$ contact. This is believed to be due to rough interface and nickel germanosilicide agglomeration in the surface of the P^+-

$Si_{0.8}Ge_{0.2}$ sample.

The characteristics of the P/N junction diodes with nickel silicide and nickel germanosilicide contacts were also studied. The contacts were formed by annealing at an optimum condition of 500℃ for 30 sec. Fig.5.12 shows the forward and reverse I-V characteristics of the nickel silicided $Si_{1-x}Ge_x$ diodes with different structures (i.e., Si/P^+-$Si_{0.8}Ge_{0.2}$, P^+-$Si_{0.8}Ge_{0.2}$, P^+-$Si_{0.7}Ge_{0.3}$). It was observed that the reverse leakage current (I_{OFF}) decreases significantly for the sample with a 25nm Si cap layer on the $Si_{0.8}Ge_{0.2}$ layer (I_{OFF} ＜ 3.5×10^{-8} A). A larger I_{OFF} for the $Si_{0.7}Ge_{0.3}$ diode is believed to be due to more nickel germanosilicide agglomerate formation on the surface. This again confirms that in order to improve the electrical characteristics of the nickel silicide contact on $Si_{1-x}Ge_x$ layer, a suitable thickness of the Si consuming layer should be grown on top of the $Si_{1-x}Ge_x$ layer for silicide formation.

5-6 Morphological stability of Ni/Si/$Si_{1-x}Ge_x$ thin films

Figure 5.13 shows the XRD spectra of nickel germanosilicide films annealed at the temperature of 350 and 500℃ for 30 sec. In addition, for the morphological stability investigation, the samples were aged at sintering temperature (400℃) with various aging times. The XRD results of a nickel germanosilicide film and nickel silicide (Si cap sample) aged at 400℃ for 48 hours is included for comparison. The formation of $Ni_3(Si_{1-x}Ge_x)_2$ at 350 ℃ and $Ni(Si_{1-x}Ge_x)$ at 500℃ was observed. It can be clearly seen that there is a shift of the particular peaks of $Ni_3(Si_{1-x}Ge_x)_2$ and $Ni(Si_{1-x}Ge_x)$ at the silicidation temperature of 350℃ and 500℃, respectively shown in Fig. 5.13. Additionally, a (111) peak of $Si_{1-x}Ge_x$ has appeared after aging at 400℃ for 48 hours. This is attributed to the segregation of Ge at agglomerate boundaries of nickel germanosilicides and subsequent formation of Ge-rich $Si_{1-x}Ge_x$. The latter was confirmed by the TEM/EDS analysis that will be discussed later in this section. As Ge concentration decreases in the nickel germanosilicides agglomerates, its

lattice constant becomes smaller this leads a shift in the peaks values.

In our previous study, the Ni/$Si_{0.8}Ge_{0.2}$ samples were reacted at 500℃ for 30s, the nickel germanosilicide agglomeration occurred and the average agglomeration size was about 100nm. However, after 48 hours aging the agglomeration size reduced concurrently with Ge segregation around the agglomerates as shown in the plane-view high-resolution TEM (HRTEM) micrographs in Fig. 5.14 (a). The average size of the agglomerates is about 8nm for the 48 hours aged sample. We conjecture that nickel in the nickel germanosilicide agglomerates and keep on reacting with the nearby $Si_{1-x}Ge_x$ during the aging process, which causes the agglomerate size reduced while Ge segregated. From the cross-section TEM/EDS analysis in Fig.5.14 (b), the labeled 4 is deficient in Ge and its chemical composition (Ni:Si:Ge=40.4:55.6:4.1) is inhomogeneous presumably because of the incomplete reactions between Ni and $Si_{0.8}Ge_{0.2}$. The chemical composition of the nickel germanosilicide film was Ni:Si:Ge=38.8:46.9:14.3 for the point labeled 3. The Ge segregation apparently appeared at the interface with the chemical composition Ni:Si:Ge=16.3:44.9:38.8 and Ni:Si:Ge=14.1:38.4:47.5, respectively for the points labeled 1 and 2 in Fig. 5.14 (b). This is because the Ge atoms tend to diffuse to the interface and the grain boundaries of the silicide layers and segregate [15,16]. In the Ni/Si/$Si_{0.8}Ge_{0.2}$ aged sample, the silicide films were found to be continuous with a smooth interface with $Si_{0.8}Ge_{0.2}$ as revealed in the plane-view TEM and cross-section TEM (XTEM) images shown in Figs. 5.14 (b) and (c). No Ge segregation was detected from the analysis of plane-view TEM/EDS direct image and the chemical composition of nickel germanosilicide was Ni:Si=48:52. However, less Ge segregation at the interface between Ni silicide and $Si_{0.8}Ge_{0.2}$ layer was detected from the analysis of cross-section TEM/EDS direct image and the chemical composition of the nickel germanosilicide was Ni:Si:Ge=3:70:27 as shown in Fig.5.14 (d). The results indicated that sample at long ageing time induced less Ge segregation and resulted in small-grained nickel silicide formation, which in turn enhances the interfacial roughness and reduces the

morphological stability of the nickel silicide.

Figure 5.15 presents the effect of the silicidation temperature on the contact resistivity of the nickel silicide (ρ_{Cns}) and the nickel germanosilicide contacts (ρ_{Cngs}) formed. After annealing at 350℃-400℃ for 30 s, the ρ_{Cngs} and ρ_{Cns} were larger than that of both ρ_C values formed at 500℃, this is because when annealed at lower temperatures (＜400℃), it formed nickel rich phase as shown in Fig.5.13. The contact resistivities reach a minimum after annealing at 500℃, the formed phases was NiSi and Ni($Si_{1-x}Ge_x$) which causes the ρ_{Cns} and ρ_{Cngs} exhibit minima of 9.56×10^{-7} and 2.23×10^{-6} Ω-cm^2 , respectively. After annealing at temperatures higher than 500℃, ρ_{Cngs} exceeded ρ_{Cns}, because the 25 nm Si cap sample which provided adequate Si for formation of nickel silicide with less agglomeration. Both ρ_{Cns} and ρ_{Cngs} increase with increasing silicidation temperature; this is due to the phase transformation [14]. The ρ_{Cngs} increased rapidly and far exceeded ρ_{Cns} at 800℃ which was the result of the new phase formation and serious agglomeration.

Figure 5.16 plots the thermal stability of the silicidation contacts aged at 400℃ with various aging time. The ρ_{Cns} remained unchanged at 400℃, while ρ_{Cngs} increased slightly after 24 hours of aging, and more rapidly to a final value of 5.18×10^{-6} Ω-cm^2. The increase in ρ_{Cngs} is associated with Ge segregation and the formation of rough interface between the nickel germanosilicide layer and $Si_{1-x}Ge_x$.

The characteristics of the *P/N* junction diodes with nickel silicide and nickel germanosilicide contacts after aging were also investigated. The contacts were formed under optimum silicidation conditions of 500℃ for 30s. Figure 5.17 presents the forward and reverse I-V characteristics of nickel silicided $Si_{1-x}Ge_x$ diodes with two different structures (Si/P^+-$Si_{0.8}Ge_{0.2}$, P^+-$Si_{0.8}Ge_{0.2}$) after aging at 400℃ for 48 hours. The reverse leakage current (I_{OFF}) of the sample with a 25 nm Si sacrificial layer on the $Si_{0.8}Ge_{0.2}$ layer (I_{OFF} ＜ 5.8×10^{-9} A) was observed to increase slightly. A larger I_{OFF} of the $Si_{0.8}Ge_{0.2}$ diode after aging is believed to be caused by the rough interface between germanosilicide and the $Si_{0.8}Ge_{0.2}$ layer

and greater Ge segregation in the $Si_{1-x}Ge_x$ layer. This result again verifies that, a suitably thick Si sacrificial layer should be grown on top of the $Si_{1-x}Ge_x$ layer during silicide formation to improve the morphological stability of the nickel silicide contact on $Si_{1-x}Ge_x$ layer.

5-7 Conclusions

We have studied the material and electrical properties of the nickel germanosilicide contact on $Si_{1-x}Ge_x$ layer. Low sheet resistances of 6.85-7.57Ω/□ were obtained for the P^+-$Si_{0.8}Ge_{0.2}$ samples annealed at 450 to 650℃. Low contact resistance of 0.97μΩ-cm^2 was obtained on the P^+-$Si_{0.91}Ge_{0.09}$ sample which was due to small grain size of agglomerates (0.1μm) and good surface coverage (85%). The $Ni_2(Si_{1-x}Ge_x)$, $Ni(Si_{1-x}Ge_x)$ and $Ni(Si_{1-x}Ge_x)_2$ phase formed after annealing at 350, 500 and 750℃ for 30 sec respectively. The grain size of the agglomerates increases with the increase of the Ge fraction, and this induced the high sheet resistance and specific contact resistance of the nickel germanosilicide contacts. In additionally, the thermal stability of the polycrystalline $Ni/(Si_{0.8}Ge_{0.2})_2$ on BF_2^+, B^+, P^+ and As^+-implanted has also been studied by sheet resistance measurements. The BF_2^+-implanted sample has good thermal stability than samples implanted with other species. The observation suggests that this is due to better morphology and microstructure for the BF_2^+-implanted sample.

We have demonstrated that in order to improve the sheet resistance, specific contact resistivity and junction leakage current of the nickel silicide contact on $Si_{1-x}Ge_x$ layer, a Si consuming layer with an appropriate thickness should be grown on the top of the $Si_{1-x}Ge_x$ layer for silicide formation. Low sheet resistance of 4.75-5.75Ω/□, low specific contact resistivity of 0.42 $\mu\Omega$-cm^2 and low junction leakage current of 3.5×10^{-8} A were obtained on the Si/P^+-$Si_{1-x}Ge_x$ sample with a 25nm Si consuming layer in our study. Besides, stable and low specific contact resistivity and junction leakage current nickel silicide Ohmic contacts have been successfully grown on $Si_{0.8}Ge_{0.2}$ layers with a 25nm sacrificial Si interlayer. The

silicidation film is uniform with a smooth interface, free from Ge segregation, thermally stable after aging at 400℃ for 48 hours. The high quality nickel silicide contact technology developed in this study can be used for the base contact technology of SiGe HBTs and for the Ohmic contacts for the SiGe raised source/drain technology in deep submicron MOSFETs.

5-8 References

[1] J. Eberhardt and E. Kasper, "Ni/Ag metallization for SiGe HBTs using a Ni silicide contact," *Semicond. Sci. Technol.* **16,** L47 (2001).

[2] Hiroshi Iwai, Tatsuya Ohguro, Shun-ichiro Ohmi, "NiSi salicide technology for scaled CMOS," *Microelectronic Engineering* **60**, 157 (2002).

[3] R. D. Thompson, K. N. Tu, J. Angillelo, S. Delage, S. S. lyer, *J. Electrochem.* Soc. **135,** 3161 (1988).

[4] J. S. Luo, W. T. Lin, C. Y. Chang, W. C. Tsai, "Pulsed KrF laser annealing of Ni/$Si_{0.76}Ge_{0.24}$ films," *J. Appl. Phys.* **82,** 3621 (1997).

[5] W. J. Chen and L. J. Chen, "Removal of end-of-range defects in BF_2^+ implanted (111)Si by the grain growth of thin NiS_2 overlayer," *J. Appl. Phys.* **69**, 7322 (1991).

[6] W. J. Chen and L. J. Chen, "Interfacial reactions of nickel thin films on BF_2^+-implanted (001)Si," *J. Appl. Phys.* **70**, 2628 (1991).

[7] D.-X. Xu, S. R. Das, C. J. Peters, and L. E. Erickson, "Material aspects of nickel silicide for ULSI applications," *Thin Solid Films* **326** ,143 (1998)

[8] L. P. Chen, C. T. Chou, G. W. Huang, and C. Y. Chang, "Boron incorporation in $Si_{1-x}Ge_x$ films grown by ultrahigh vacuum chemical vapor deposition using Si_2H_6 and GeH_4," *Appl. Phys. Lett.* **67**, 3001 (1995).

[9] J. S. Luo, W. T. Lin, C. Y. Chang, and P. S. Shih, "Interfacial reactions of Ni/$Si_{0.76}Ge_{0.24}$ and Ni/$Si_{1-x-y}Ge_xC_y$ by vacuum annealing and pulsed KrF laser annealing," *Nuclear Instruments and Methods in Physics Research B* vol. **169**, 124 (2000).

[10] W. J. Chen and L. J. Chen, "Thermal stability of $NiSi_2$ on high-dose ion-implanted (001) Si," *J. Appl. Phys.* **71**, 653 (1992).

[11] W. Lur and L. J. Chen, "Interfacial reactions of titanium thin films on BF_2^+ -implanted (001)Si," *J. Appl. Phys.* **66**, 3604 (1989).

[12] D.-X. Xu, S. R. Das, C. J. Peters, L. E. Erickson, "Material aspects of nickel silicide for

ULSI applications," *Thin Solid Films*, vol.**326**, 143 (1998).

[13] A. Lauwers, P. Besser, T. Gutt, A. Satta, M. de Potter, R. Lindsay, N. Roelandts, F. Loosen, S. Jin, H. Stucchi, C. Vrancken, B. Deweerdt, K. Maex, "Comparative study of Ni-silicide and Co-silicide for sub 0.25-μm technologies," *Microelectronic Engineering* vol. **50**, 103 (2000).

[14] J. S. Luo, W. T. Lin, C. Y. Chang, and P. S. Shih, " Interfacial reactions of $Ni/Si_{0.76}Ge_{0.24}$ and $Ni/Si_{1-x-y}Ge_xC_y$ by vacuum annealing and pulsed KrF laser annealing," *Nuclear Instruments and Methods in Physics Research B* vol. **169**, 124 (2000).

[15] H. J. Huang, K. M. Chen, C. Y. Chang, T. Y. Huang, T. C. Chang, L. P. Chen, and G. W. Huang, "Study of boron effects on the reaction of Co and $Si_{1-x}Ge_x$ at various temperatures," *J. Vac. Sci. Technol. A* **18**, 1448 (2000)

[16] W. W. Wu, T. F. Chiang, S. L. Cheng, S. W. Lee, Y. H. Peng, H. H. Cheng, and L. J. Chen, "Enhanced growth of $CoSi_2$ on epitaxial $Si_{0.7}Ge_{0.3}$ With a sacrificial amorphous Si interlayer," *Appl. Phys. Lett.* Vol. **81**, No. 5, 2002

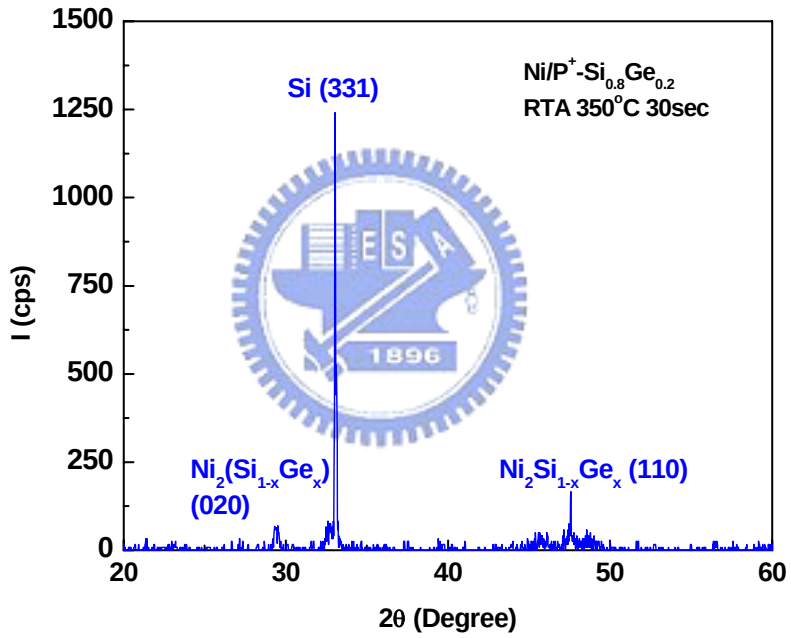

Fig.5.1 (a) XRD spectra of he $Ni_2(Si_{1-x}Ge_x)$ phase annealed at the temperature of 350℃ for 30 sec.

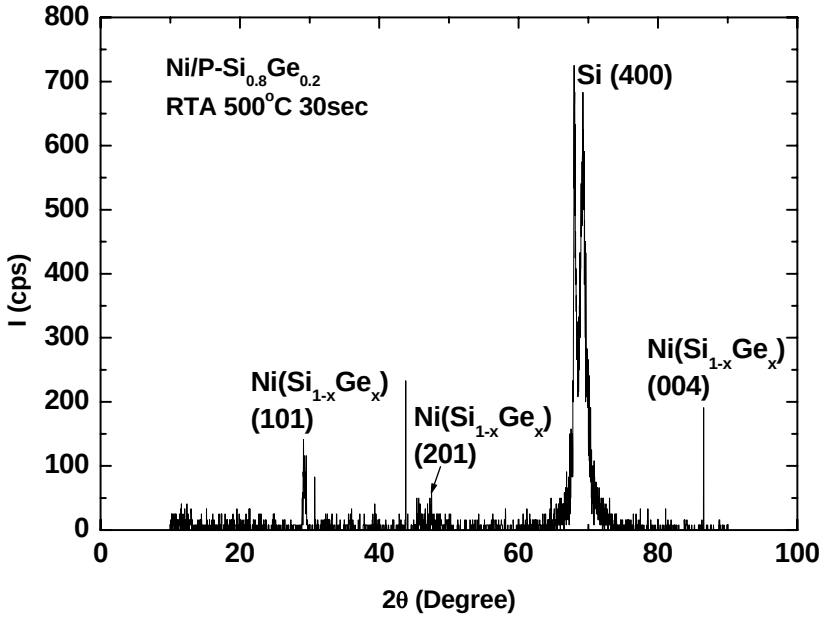

Fig.5.1 (b) XRD spectra of the Ni ($Si_{1-x}Ge_x$) phase annealed at the temperature of 500℃ for 30 s.

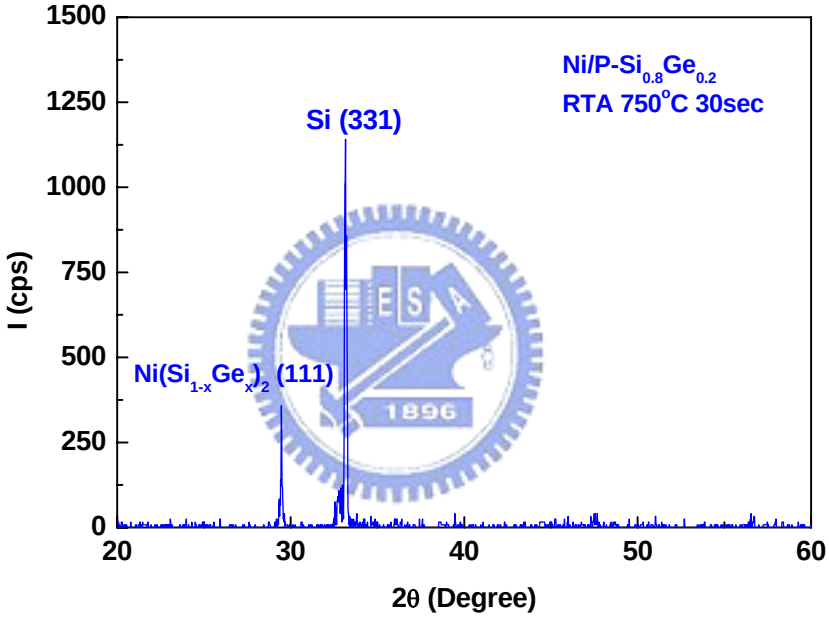

Fig.5.1 (c) XRD spectra of the Ni $(Si_{1-x}Ge_x)_2$ phase annealed at the temperature of 750℃ for 30 s.

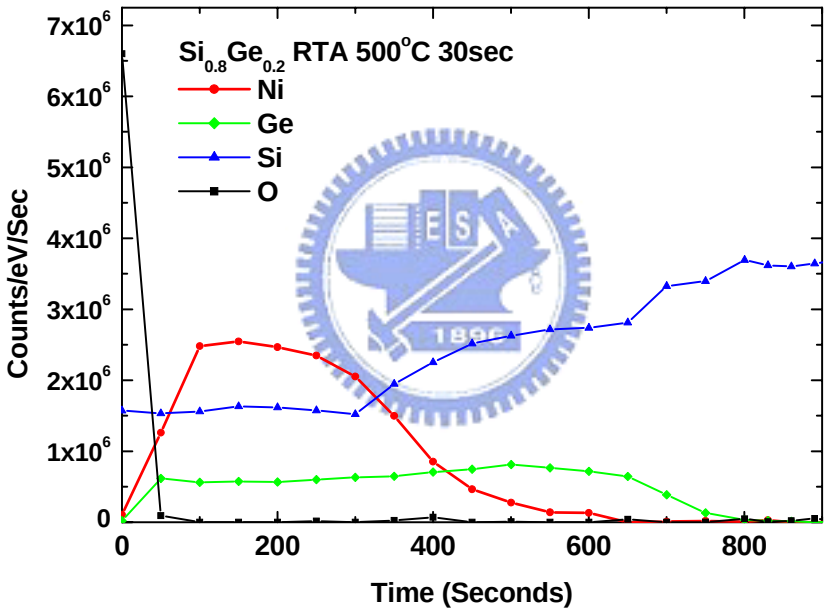

Fig.5.2 (a) AES depth profiles of the Ni/$Si_{0.8}Ge_{0.2}$ sample after annealing at 500 ^{o}C for 30 s.

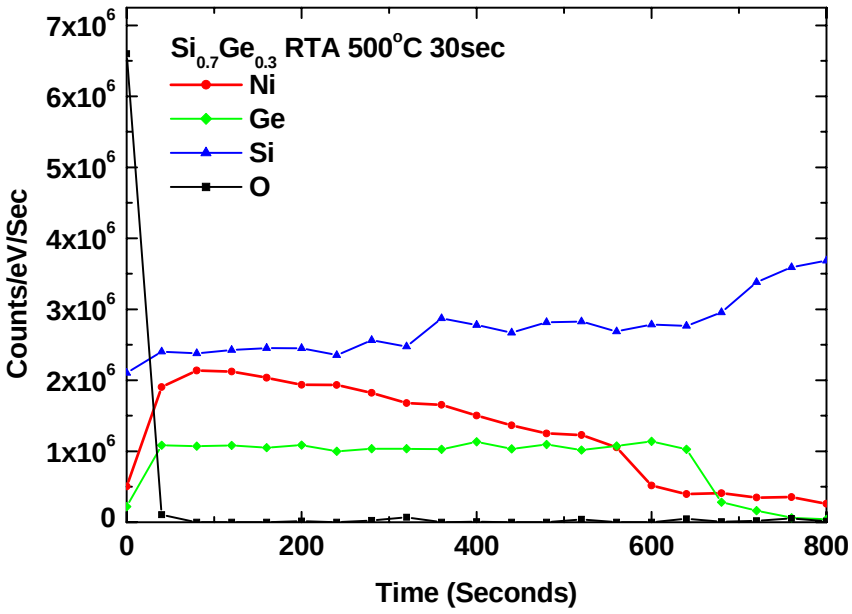

Fig.5.2 (b) AES depth profiles of the Ni/$Si_{0.7}Ge_{0.3}$ sample after annealing at 500 ^{o}C for 30 s.

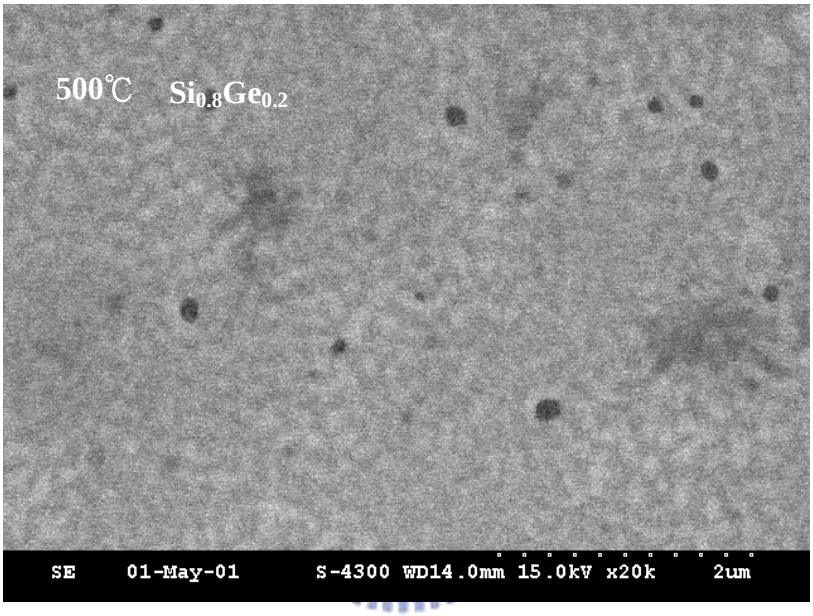

Fig.5.3(a) Scanning electron microscopy micrographs of the surface morphology of the $Ni/Si_{0.8}Ge_{0.2}$ sample after annealing at 500 ℃ for 30 sec.

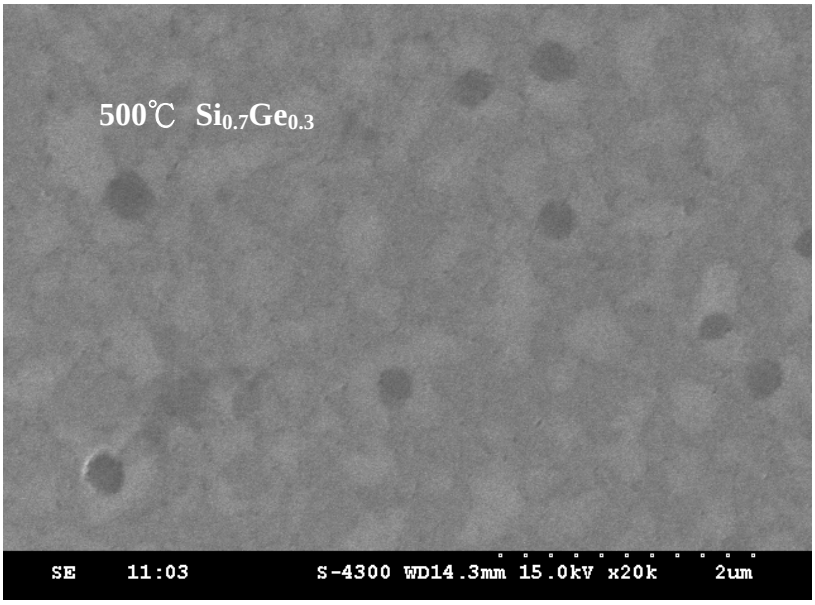

Fig.5.3 (b) Scanning electron microscopy micrographs of the surface morphology of the Ni/$Si_{0.7}Ge_{0.3}$ after annealing at 500 ℃ for 30 s.

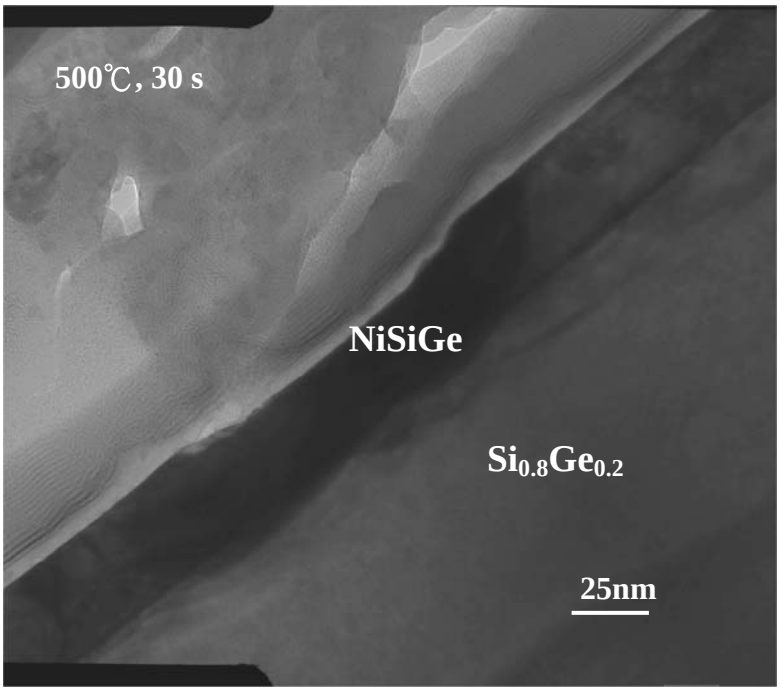

Fig.5.4 (a) Cross-section TEM micrograph of the 500℃, 30s annealed P^+-$Si_{0.8}Ge_{0.2}$ sample.

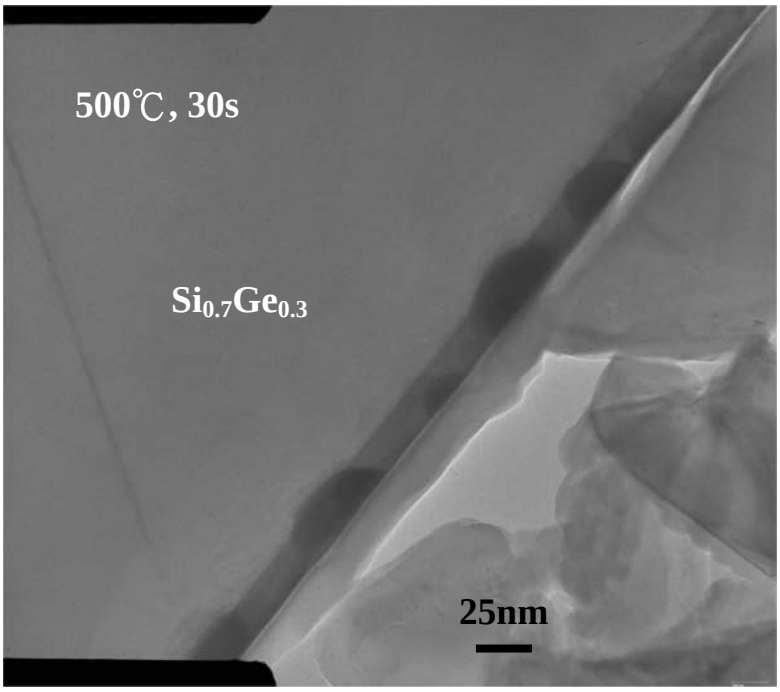

Fig.5.4 (b) Cross-section TEM micrograph of 750℃, 30s annealed P^+-$Si_{0.7}Ge_{0.3}$ sample.

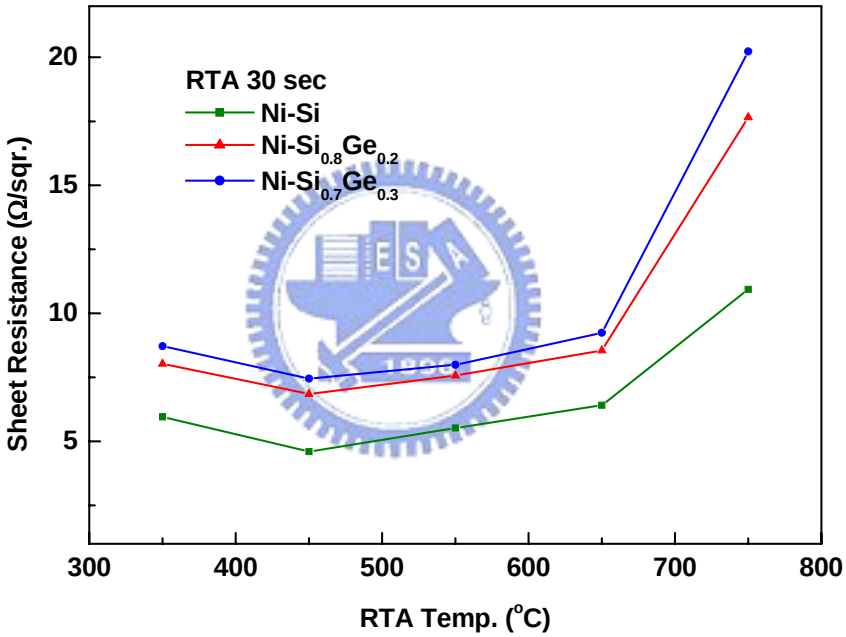

Fig.5.5 Sheet resistance comparison of the annealed Ni silicide and Ni germano-silicide for the Ni/PSi, Ni/$P^{+}Si_{0.8}Ge_{0.2}$ and Ni/$P^{+}Si_{0.7}Ge_{0.3}$ samples.

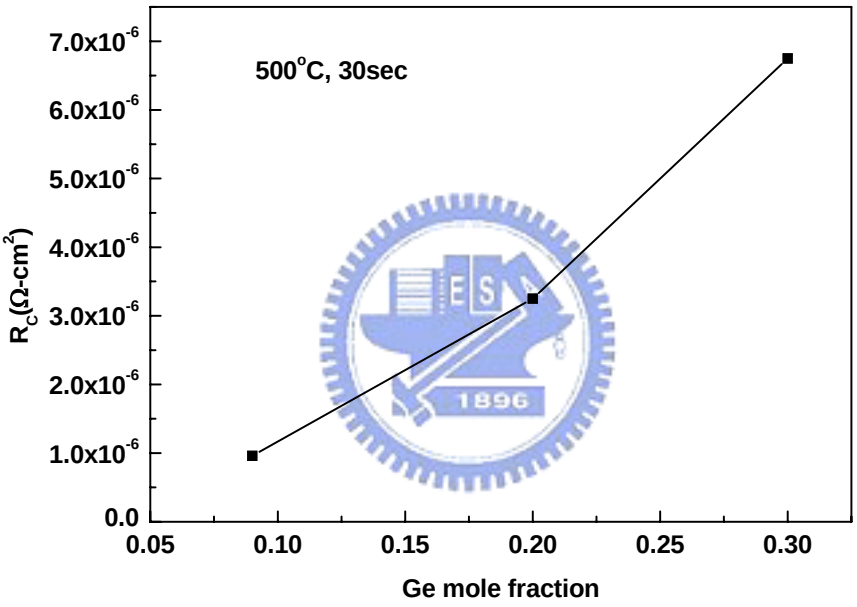

Fig.5.6 The contact resistance as a function of Ge mole fraction. Measured using TLM pattern.

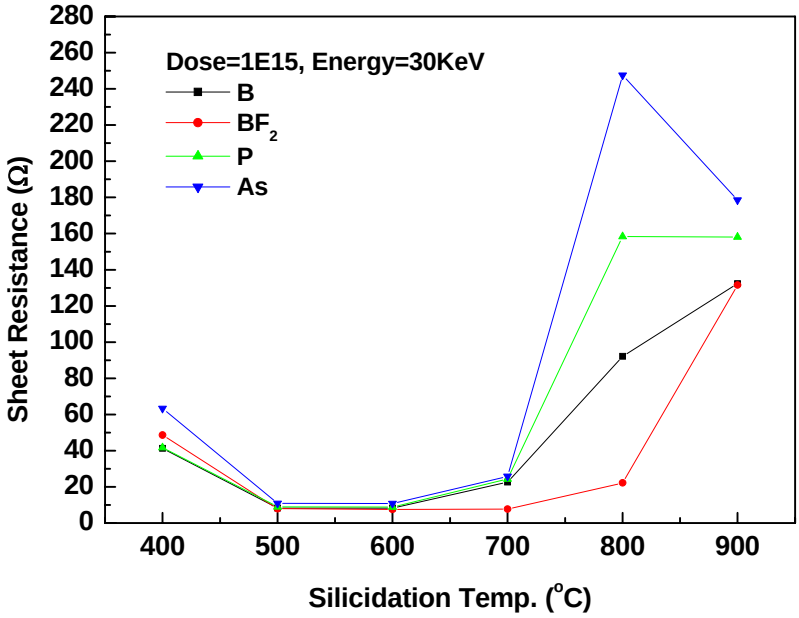

Fig.5.7 Sheet resistance vs silicidation temperature for $Ni/Si_{0.8}Ge_{0.2}$ on various ion-implanted samples.

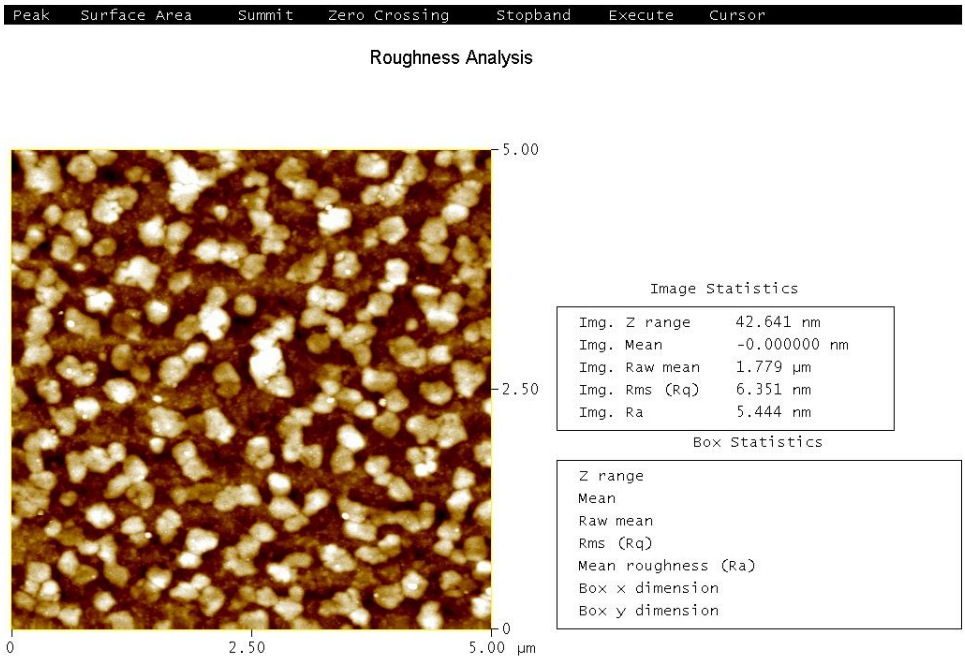

(a) As^{+}-implanted sample

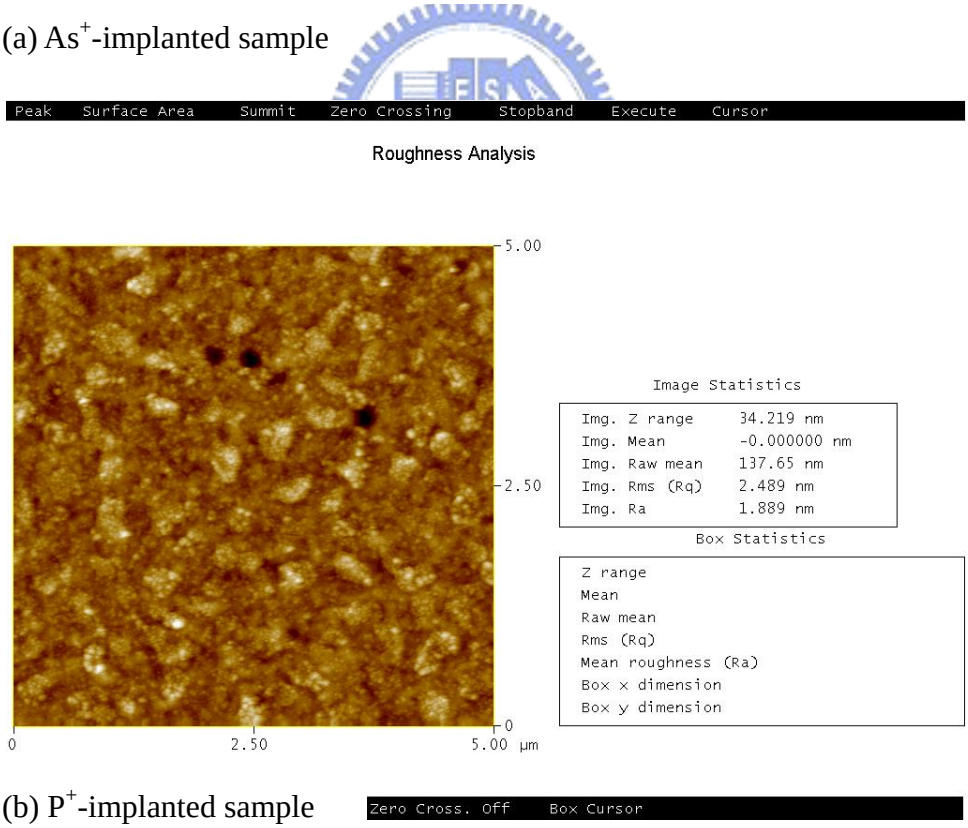

(b) P^{+}-implanted sample

Fig.5.8 Surface morphology of the (a) As^{+} and (b) P^{+} implanted samples after annealing at 800℃ for 30s.

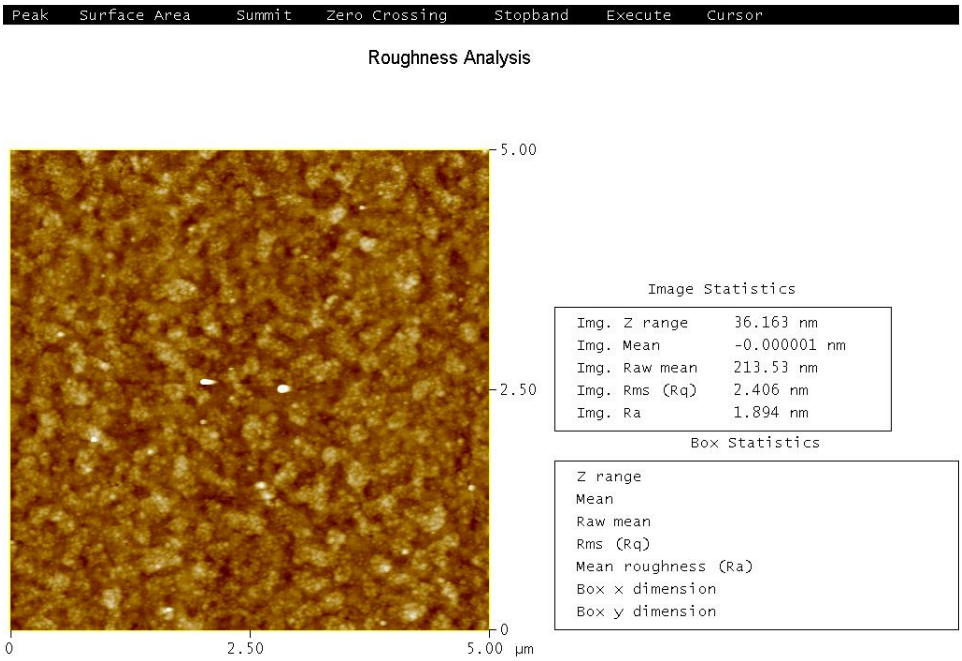

(c) B^+-implanted sample

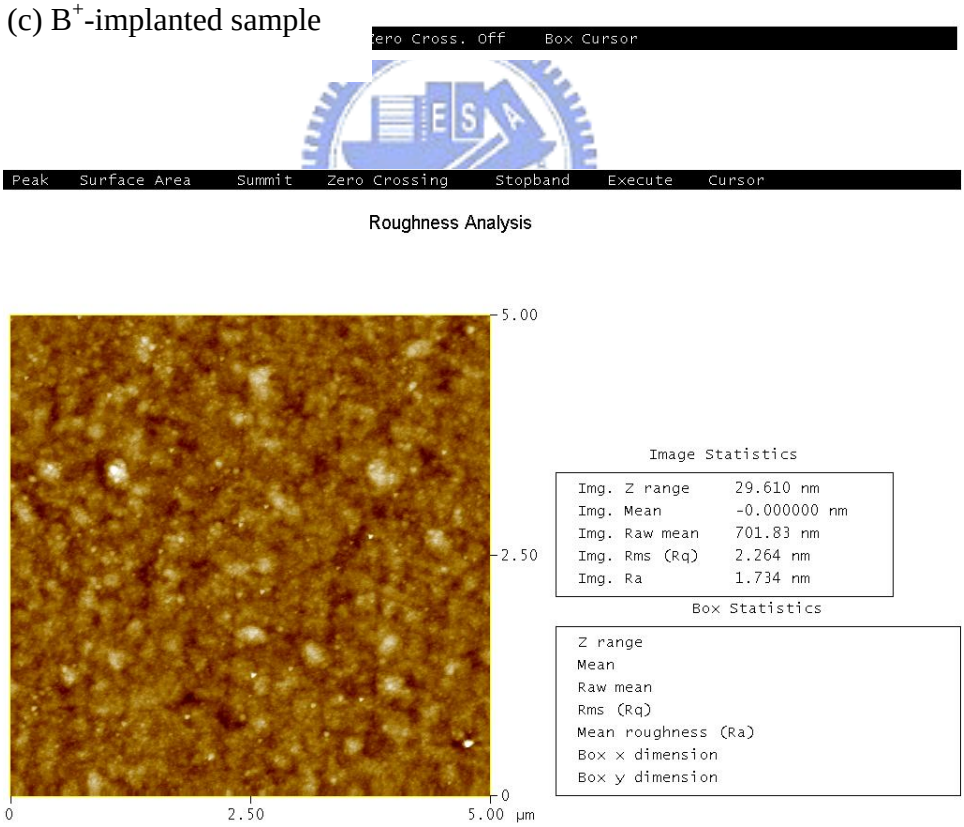

(d) BF_2^+-implanted sample

Fig.5.8 Surface morphology of the (c) B^+ and (d) BF_2^+ implanted samples after annealing at 800℃ for 30s.

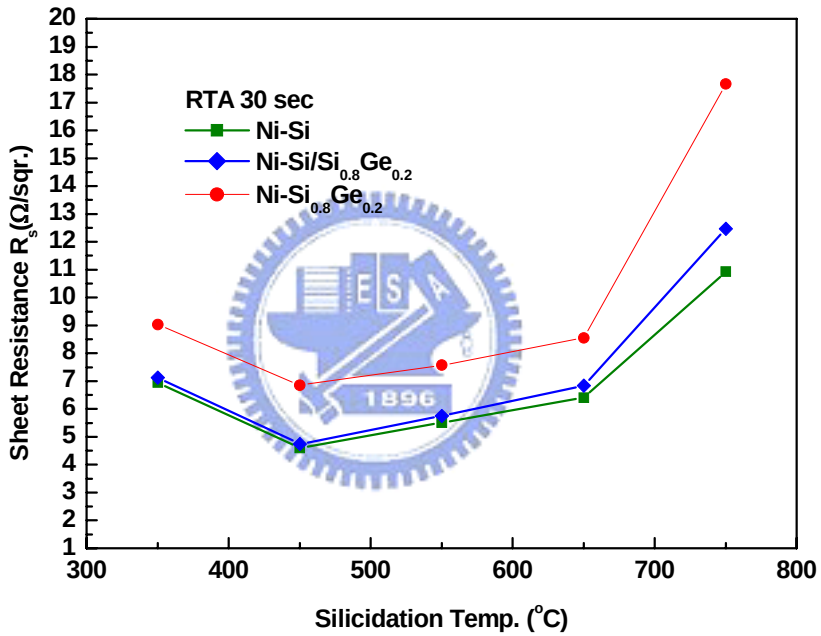

Fig.5.9 Sheet resistances comparison of the annealed Ni silicide and Ni germano-silicide for P-Si, Si/P^+-$Si_{0.8}Ge_{0.2}$ and P^+-$Si_{0.8}Ge_{0.2}$ samples.

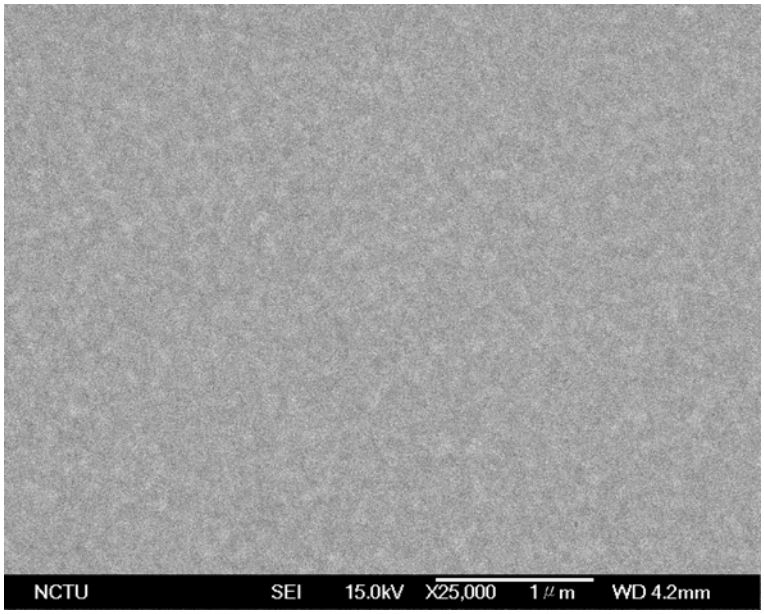

Fig.5.10 (a) SEM micrographs of the surface morphology of the Ni/Si/$Si_{0.8}Ge_{0.2}$ sample annealed at 500 ℃ for 30 sec.

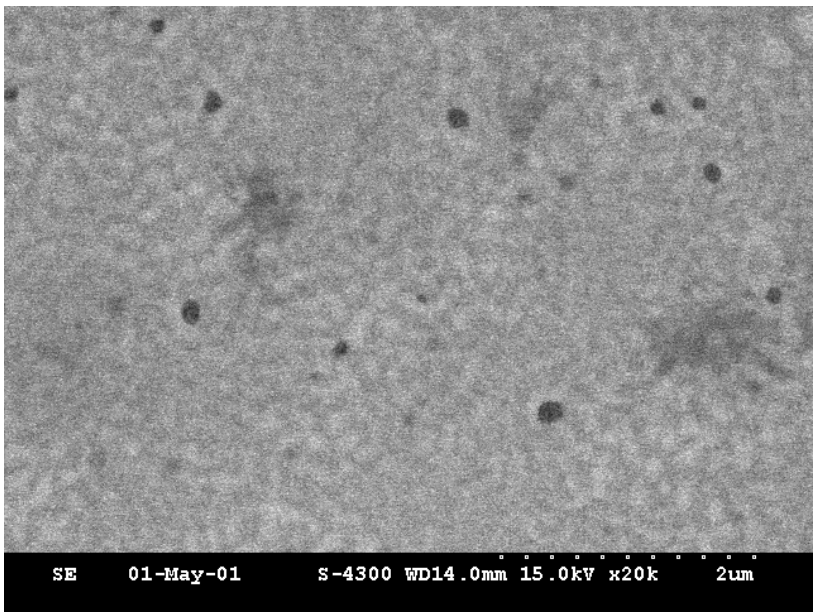

Fig.5.10 (b) SEM micrographs of the surface morphology of the $Ni/Si_{0.8}Ge_{0.2}$ sample annealed at 500 ℃ for 30 sec.

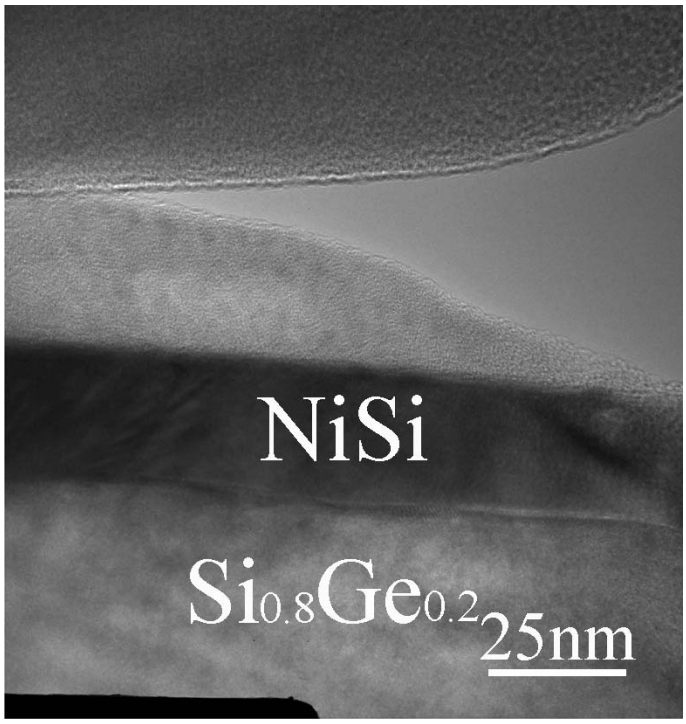

Fig.5.10 (c) Cross-section TEM of Ni/Si/$Si_{0.8}Ge_{0.2}$ sample annealed at 500℃ for 30 sec.

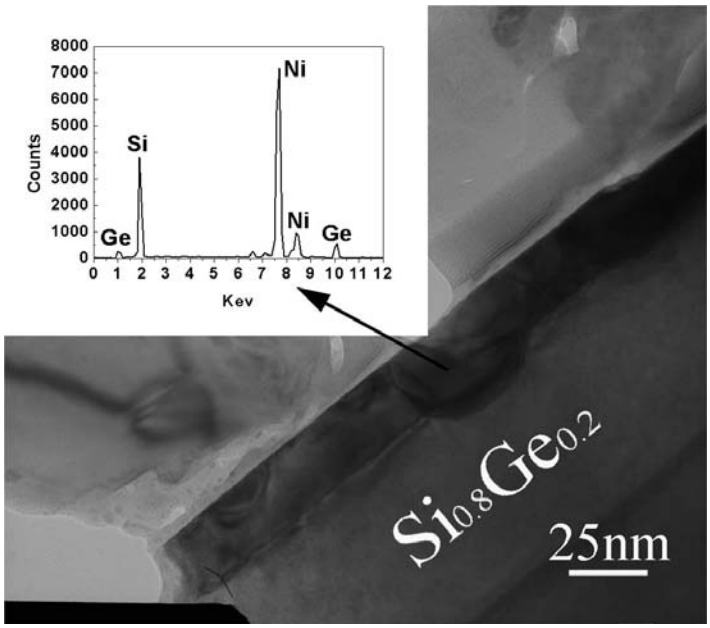

Fig.5.10 (d) Cross-section TEM of Ni/$Si_{0.8}Ge_{0.2}$ sample annealed at 500℃ for 30 sec.

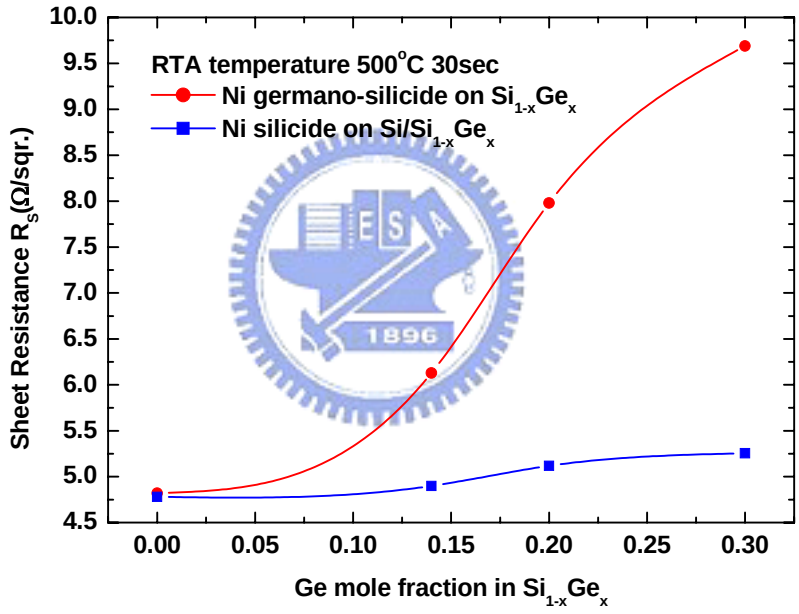

Fig.5.11 Sheet resistance as a function of Ge mole fraction for 25 nm Si capping layer and P^{+}-$Si_{1-x}Ge_x$ layer after annealing at 500℃ for 30 sec.

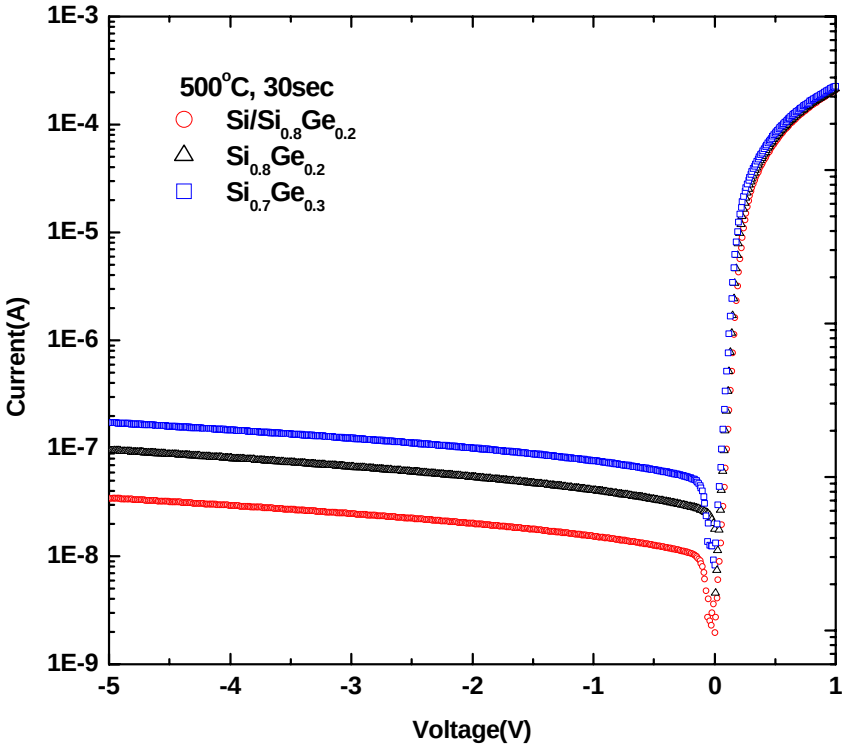

Fig.5.12 The forward and reverse characteristics for the $Si/Si_{0.8}Ge_{0.2}$, $Si_{0.8}Ge_{0.2}$, $Si_{0.7}Ge_{0.3}$ P^{+}-N junction.

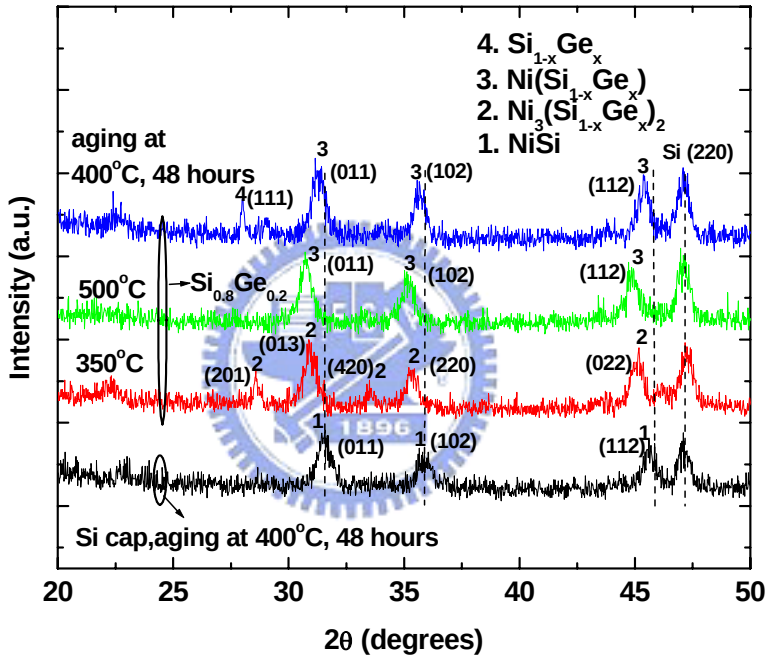

Fig.5.13 XRD spectra of nickel germanosilicide films annealed at different temperature for 30 sec. XRD spectra of nickel silicide and germanosilicide films aged at 400℃ for 48 hours are also included for comparison.

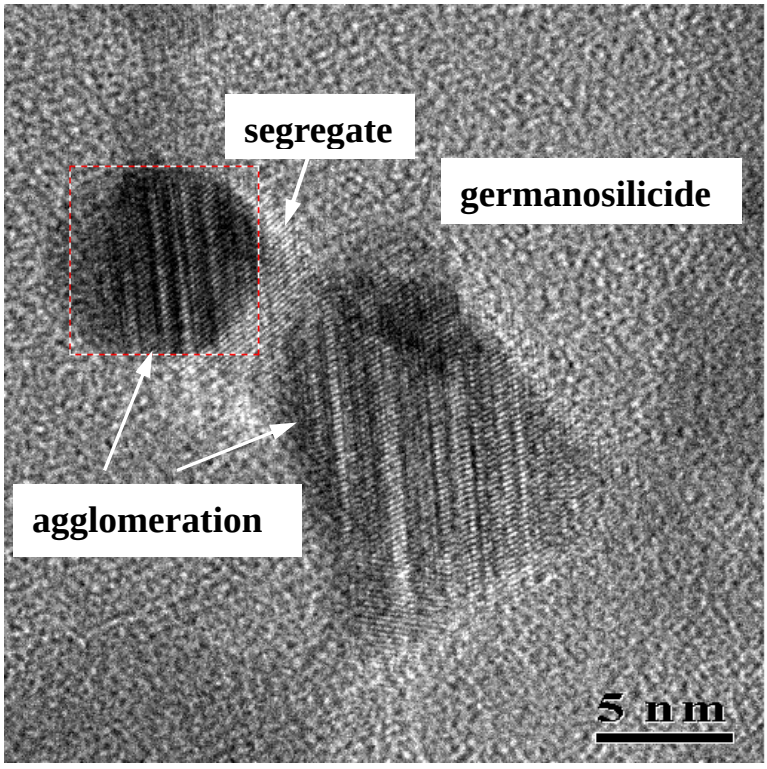

Fig.5.14 (a) Plane-view HRTEM micrograph for the Ni/$Si_{0.8}Ge_{0.2}$ aged sample.

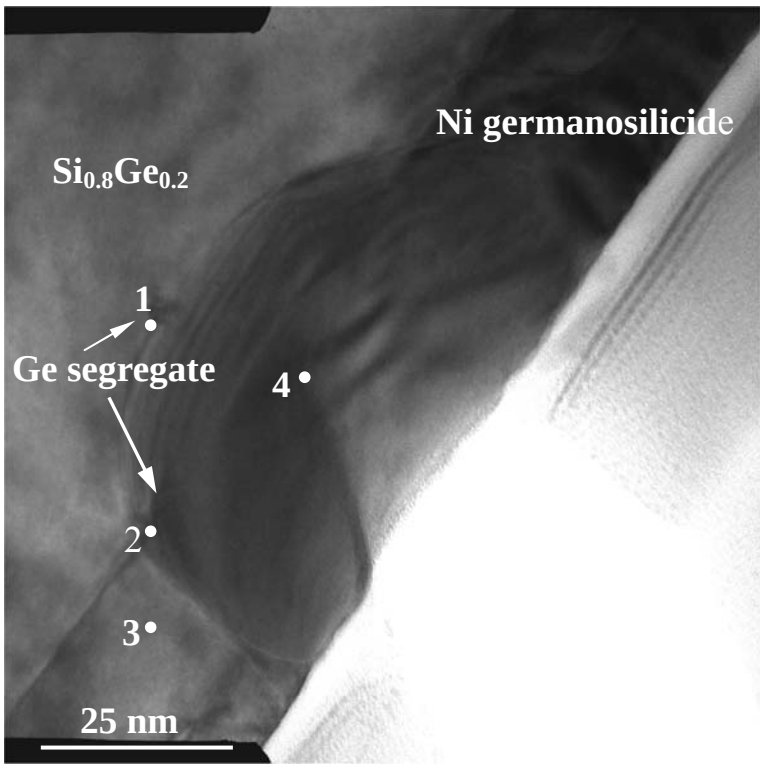

Fig.5.14 (b) shows the cross-section TEM/EDS analysis.

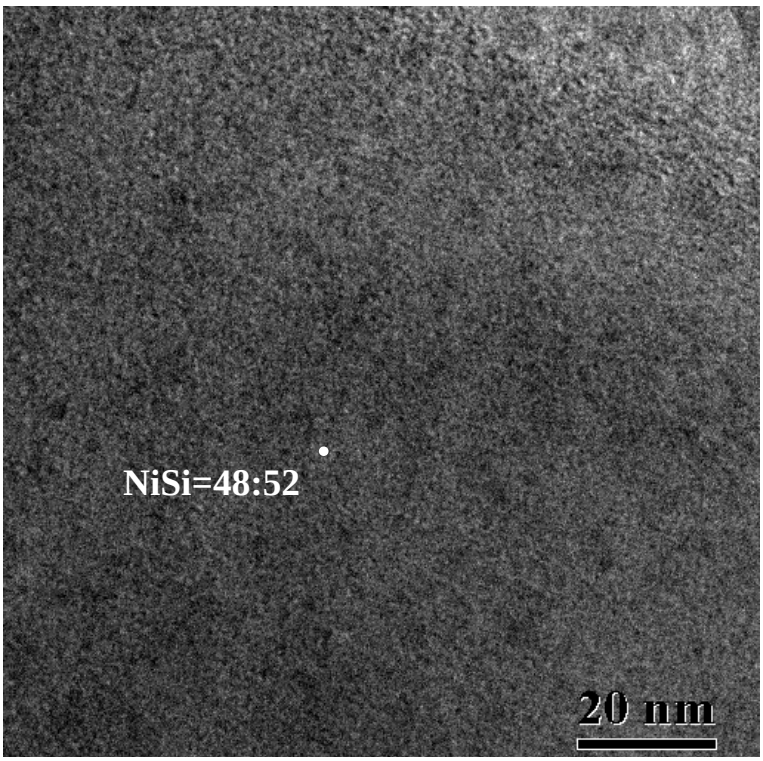

Fig.5.14 (c) shows the plane-view TEM image for the Ni/Si/$Si_{0.8}Ge_{0.2}$ aged sample.

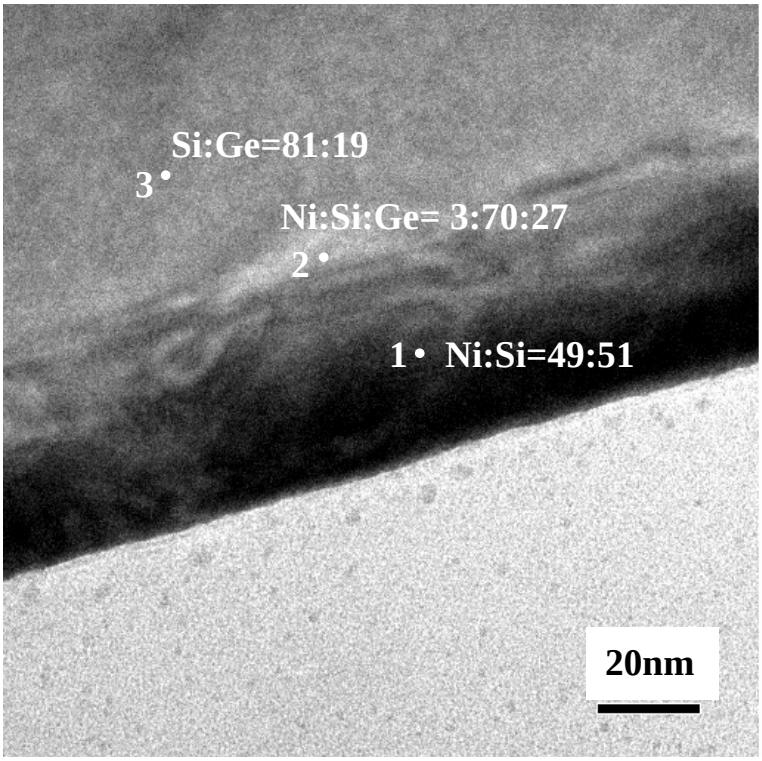

Fig.5.14 (d) Less Ge segregation at the interface between Ni silicide and $Si_{0.8}Ge_{0.2}$ layer was detected from the analysis of cross-section TEM/EDS direct image and the chemical composition of nickel germanosilicide is Ni:Si:Ge=3:70:27.

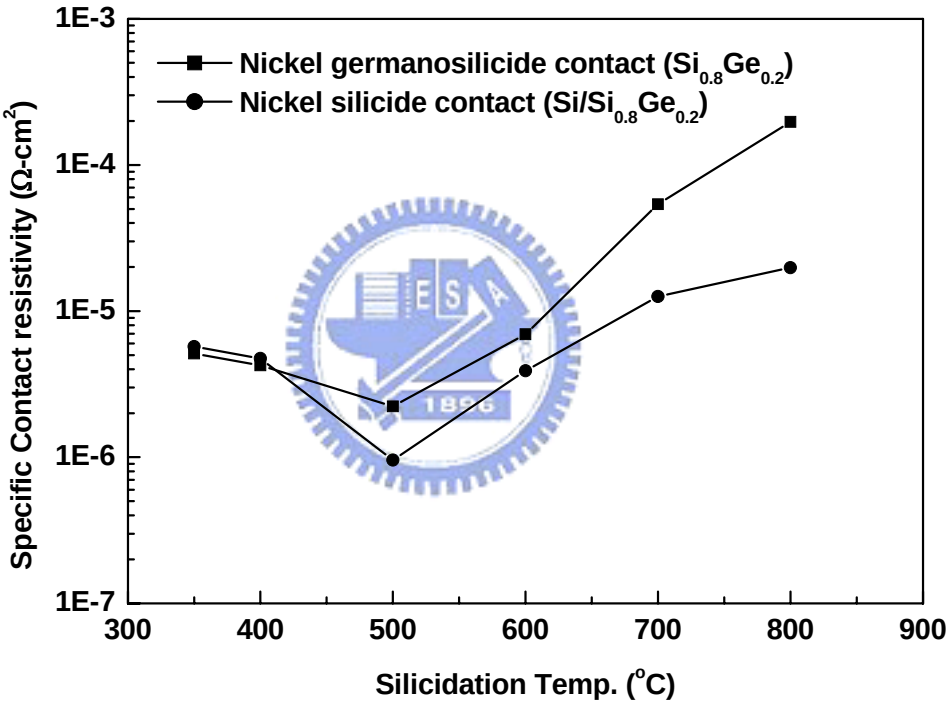

Fig.5.15 Effect of the silicidation temperature on the contact resistivity of the nickel silicide (ρ_{Cns}) and the nickel germanosilicide contacts (ρ_{Cngs}) formed.

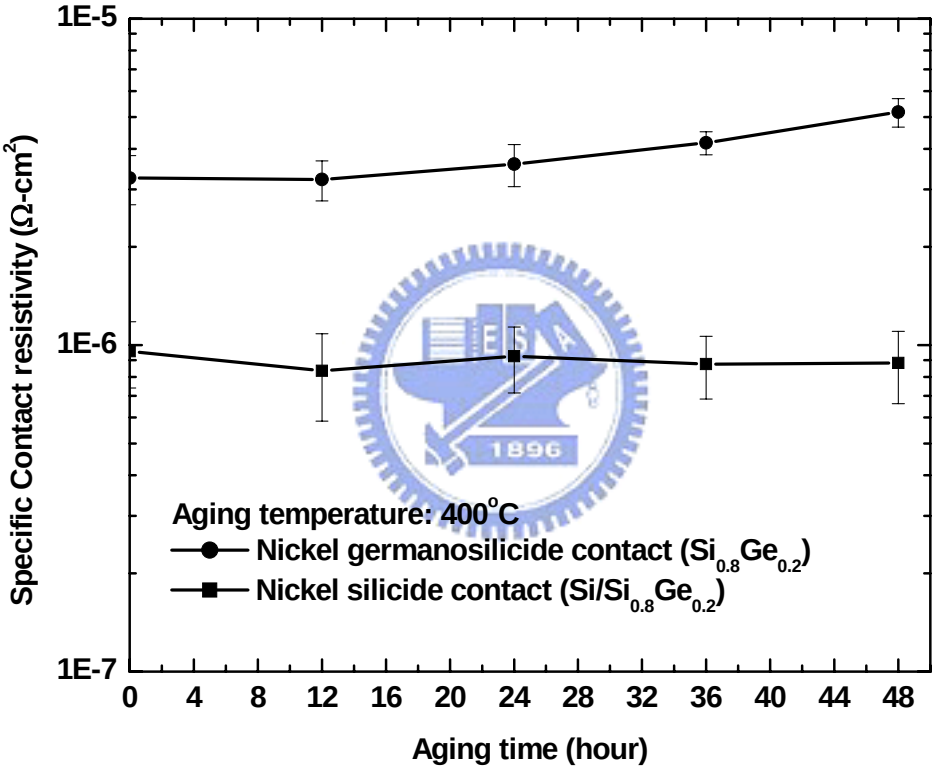

Fig.5.16 Thermal stability of the silicidation contacts after aged at 400℃ for various aging time.

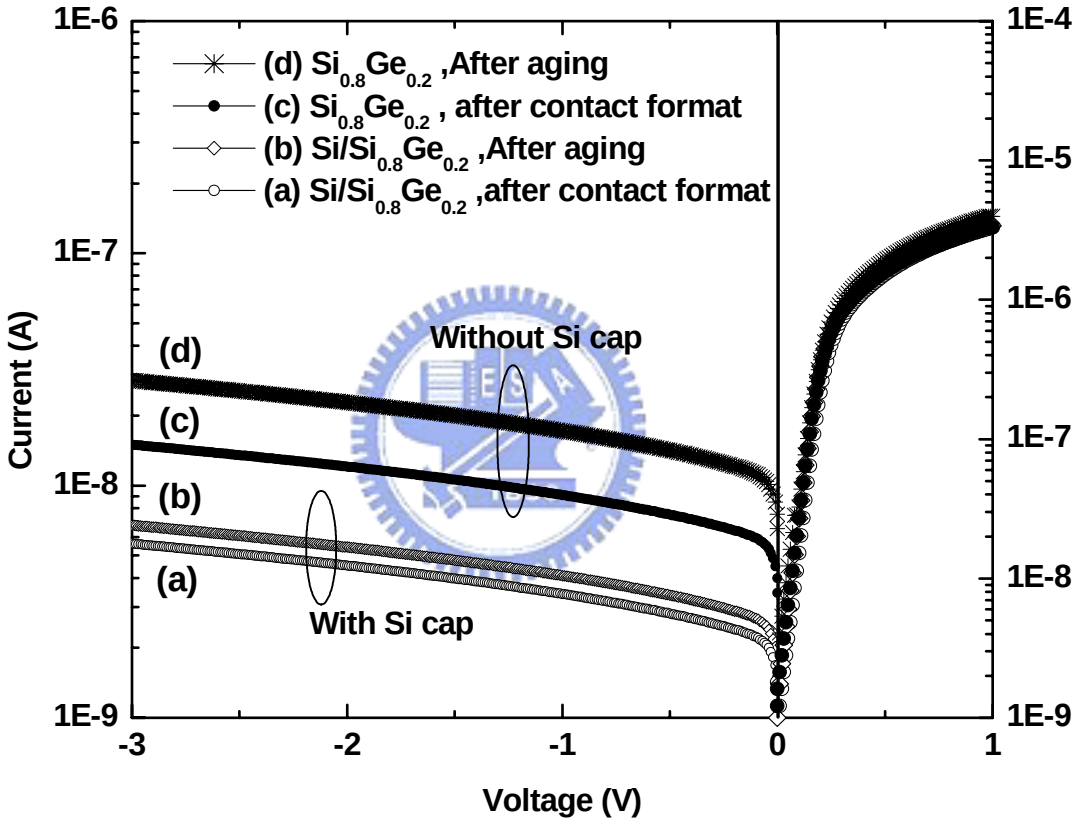

Fig.5.17 Forward and reverse I-V characteristics of the nickel silicided $Si_{1-x}Ge_x$ diodes with two different structures (Si/P^+-$Si_{0.8}Ge_{0.2}$, P^+-$Si_{0.8}Ge_{0.2}$) after aging at 400℃ for 48 hours.